

FINAL TECHNICAL REPORT

Award Number: G11AP20030

Seismological Studies of the Central Denali-Northern Foothills Fold and Thrust Belt – Fairbanks Region

Diane I. Doser

The University of Texas at El Paso

Department of Geological Sciences, 500 W. University Ave., El Paso, TX 79968

(915)-747-5851 (office), (915)-747-5073 (FAX), doser@utep.edu

Grant duration: January 1, 2011 to May 31, 2012

ABSTRACT

This research focused on historical and recent seismicity of the interior Alaska and its relationship to other geophysical and geological data sets to better understand the interactions between the central Denali fault, Northern Foothills fold and thrust belt (NFFTB), and the Fairbanks-Salcha-Minto Flats seismic zones. This region is a complicated zone of deformation that includes right-lateral strike-slip motion along the Denali fault, thrusting to the north within the NFFTB, and left-lateral strike-slip faulting within the Fairbanks, Salcha and Minto seismic zones. Regional deformation is driven in part by oblique collision between North America, the Pacific plate, and the Yakutat microplate, as well as interaction between the Wrangell and Bering microplates. The research proposed the following tasks: 1) Comparing recent and historical seismicity to known bedrock and surface geology, gravity, magnetic, tomographic, GPS and paleoseismic data to identify active faults and structures, 2) Expanding and updating analysis of historical (pre-digital) earthquake sequences, and 3) Using empirical Greens function analysis to determine the rupture directivity and stress drops of moderate earthquakes. The preliminary results of this research are outlined in the following sections.

INTRODUCTION

The focus of our study was the region of central Interior Alaska (Figure 1). Over 5 events of $M > 7$ have occurred in this region since 1900, making it the most seismically active region of Alaska outside of the Pacific-North America-Yakutat plate boundary zone. The right-lateral strike-slip Denali fault exhibits the highest slip rate of any fault within Interior Alaska (up to 13.5 mm/year; Matmon et al., 2006) and was the site of the 2002 $M_w=7.9$ Denali fault earthquake that ruptured over 220 km to the east along the fault, and then ruptured over 60 km along the Totschunda fault (Haeussler et al., 2004).

Located to the north and paralleling the Denali fault is the Kobuk-Tintina fault system (Figure 1). There is little evidence for Quaternary rupture along the system (Plafker et al., 1994) and the slip rate along the system is estimated to be < 5 mm/yr (Page et al., 1995). North to north-northeast trending, left-lateral, seismically active faults lie between the Denali and Kobuk/Tintina systems (Figures 2 and 3). These structures are the site of the $M_S=7.3$ 1937 Salcha and the 1947 $M_S=7.3$ Fairbanks Seismic zone events (red solid diamonds, Figure 2). Swarms of moderate magnitude earthquakes (5.5 to 6) have also occurred near Fairbanks (Figure

2). Several earthquakes of $M > 6$ may be associated with the Northern Foothills Fold and Thrust belt (NFFTB) located north of the Denali fault (Figure 2). Focal mechanisms from recent and historic earthquakes (Figure 2) indicate the change from thrust faulting of the NFFTB to strike-slip faulting of the Minto, Fairbanks and Salcha seismic zones occurs between 64 and 64.5°N.

Identifying active faults and structures using geophysical information

With the exception of the 2002 and 1912 earthquakes along the Denali fault, no surface faulting has been observed in any events occurring within Interior Alaska. In addition, few faults with Neogene motion have been mapped (Figure 2). However, the thick vegetation, swamps, frequent snow cover and extensive river systems of this region have made observations of such features difficult. Thus one objective of this study was to use other geophysical data to delineate geological structures that could control present day seismicity.

Gravity data for the study area (Saltus et al., 2006) are limited to observations along roads and major rivers (Figure 4). The data have reasonable coverage in the region of the 1967 Fairbanks and 1937 Salcha earthquakes, but coverage is poor in the vicinity of the 1947 event and earlier events in the NFFTB.

A comparison of Bouguer gravity anomalies to seismicity (Figure 5) indicates that the gravity data illustrate a predominantly northeast-southwest trending structural trend consistent with the seismicity. The purple lines indicate the assumed orientations and rupture lengths of earthquakes associated with the 1937, 1947 and 1967 sequences based on the studies of Fletcher and Christensen (1996), Gedney and Berg (1969) and Gedney et al. (1980, 1982). Note that the estimated rupture zone for the 1937 Salcha event appears to extend to the edges of two Bouguer anomaly lows. The Minto seismic zone appears to be concentrated within a northeast trending Bouguer anomaly low. The -50 mGal contour at the southern edge of the study area separates the east-west trending structures of the NFFTB from the Salcha, Fairbanks and Minto seismic zones.

Aeromagnetic data (Saltus et al., 1999) for the study area (Figure 6) provide a more detailed view of subsurface structures as the flight lines were more closely spaced in the study area. The northeast structural grain is most apparent within the region of the Minto seismic zone, but this structural trend is increasingly disrupted to the east by shorter wavelength features with differing strikes. The swarm activity near Fairbanks occurs between several magnetic highs, while the epicenter for the 1947 event occurs near one of the strongest magnetic highs in the region. The southwestern portion of the 1937 Salcha rupture zone bounds the edge of magnetic high. Note that the poorly determined epicenters for two magnitude 6 1/2 - 6 3/4 earthquakes occurring in 1929 (green diamonds, Figure 6) are also near the edges of magnetic highs. Magnetic lows characterize much of the NFFTB.

We performed additional filtering of the magnetic data in order to enhance deeper, long wavelength anomalies. Figure 7 shows a low pass (> 10 km wavelengths), strike filtered (only features with strikes of 30° to 60° NE passed) map of the Fairbanks and Salcha seismic zones. The rupture zone of the 1937 event (gray bold line) and recent seismicity occurs at the edge of a magnetic low (< -20 nT), with the epicenter for the 1937 mainshock located at the northeastern edge of the deepest portion (< -35 nT) of the low. Interestingly, the 1947 mainshock epicenter occurs at the southwestern edge of the deepest portion of the same low. The 1967 sequence occurs in a region of higher magnetic intensities (20-60 nT) with no distinctive surrounding lows.

A map that drapes gravity (color) over a shaded relief map of aeromagnetics (Figure 8) further highlights that both the 1937 and 1947 events nucleated in regions where magnetic anomalies are sharply terminated, suggesting some relation between their nucleation points and the underlying magnetic structure. The Minto seismic zone fills a region of relatively low magnetic relief. The map also suggests that structures of the NFFTB extend to $\sim 64.1^\circ\text{N}$.

In summary, trends in bedrock geology are revealed by both the gravity and magnetic data and that these trends suggest there are geological controls on the nucleation points, fault orientations, rupture lengths and type of faulting observed in the region. The 1937 Salcha event may have completely ruptured along the edge of the bedrock structure that controls the Salcha seismic zone. Aftershock sequences in intraplate regions (with low slip rates) can be extremely long-lived (e.g., Ebel et al., 2000), and it is likely that recent seismicity within the Salcha seismic zone may reflect continuing aftershocks of the 1937 sequence. The length of the magnetic anomaly within the epicentral region of the 1947 sequence (~ 25 km, Figure 8) suggests that the 1947 event may represent the maximum size thrust/reverse fault event for this structure. The large gravity anomaly signature associated with the Minto seismic zone and its occurrence in a region of significant disruption of the surrounding magnetic anomalies may indicate this zone is capable of nucleating large earthquakes, perhaps even larger than the 1937 Salcha event. Finally, the epicentral region of the 1967 sequence is characterized by short wavelength, complex magnetic and gravity anomalies, suggesting a lack of major through going structures, leading to the swarm-like nature of seismicity within this region. Results of this portion of our research were presented at the spring 2012 meeting of the Seismological Society of America.

Analysis of historic events

Analysis of seismograms of the 1929, 1937 and 1947 events is still ongoing. Preliminary comparisons of the seismograms of the October 15, 1947 mainshock with its largest aftershock ($M \sim 6.8$ on October 20, 1947) indicate the two events had similar mechanisms. Seismograms of the January 21, 1929 earthquake are similar to those of the 1947 mainshock, also suggesting a similar mechanism. However, comparisons of seismograms of the two 1929 events indicate the July 4 event is considerably smaller than the January 21 event, although catalogs (e.g. Alaska Earthquake Information Center) give a magnitude of 6.5 for the July event and 6.3 for the January event. A graduate student, Christopher Dankoff, will be completing analysis of these events for his MS Thesis, with an expected defense date of May 2013.

Empirical Greens Function Studies

We have analyzed the stress drops of 24 earthquakes (Tables 1 and 2) along the Denali and Totschunda fault system (Figure 9) occurring between July 2002 and November 2005 using the empirical Greens function (EGF) technique. The events include the Nenana Mountain and Denali fault mainshocks and numerous aftershocks. The EGF approach requires prior knowledge of the events' seismic moments. We used M_w , when available, to estimate the mainshock-EGF magnitude difference and select the EGF pairs. For most events in our data set the Alaska Earthquake Information Center (AEIC) reports seismic moment, M_0 , and moment magnitude, M_w , that was used for our calculations. When the seismic moment was not available from the AEIC, we used local magnitude, M_L , or the moment magnitude, M_w , reported by IRIS to estimate the seismic moment (Escudero and Doser, 2012).

The EGF approach also requires local estimates of seismic velocity and density. In this study we use the values given by Brocher et al. (2004) from results of active seismic reflection/refraction experiments conducted along the central Denali fault in 1986 and 1987.

To estimate the stress drop we use smaller earthquakes as EGF along with the water level deconvolution technique to determine the larger (mainshock) earthquakes' relative source time functions (RSTFs). This technique has been widely used and described in detail by many authors (e.g. Ammon et al., 1993; Velasco et al., 1994; Escudero and Doser 2012). First, we deconvolve the EGF from the mainshock seismogram at a particular station. The EGF is an earthquake that captures the essential aspects of path and recording site relevant to the mainshock (i.e. has a similar location, centroid depth, and focal mechanism, recorded at the same station with the same instrument, and is at least one magnitude unit smaller than the mainshock, but should be large enough to be recorded with high signal-to-noise ratio by a reasonable number of stations) ensuring that the duration of the EGF is shorter than the mainshock (Mueller, 1985). Ideally, a foreshock or aftershock is a suitable EGF, but any event occurring in the area and meeting the above criteria can be used.

To perform the analysis we first manually pick the P-phase of both the mainshock and the EGF, pad the traces with zeros, remove the seismogram mean and trend, apply a Hanning window to taper the seismogram near the ends, and apply a fast Fourier transform (FFT) to obtain its complex frequency spectra. Then to accomplish the deconvolution, we divide the mainshock by the EGF frequency spectrum; the quotient represents the mainshock RSTF spectrum, scaled to the EGF seismic moment. Next, we apply a bandpass filter (0 to 1 Hz) to stabilize the deconvolution by eliminating high-frequency noise and filtering out frequencies meaningless to the result. Finally, we apply an inverse fast Fourier transformation (IFFT) to the corrected spectral quotient to generate a time series that represents the RSTF of the mainshock scaled to the seismic moment of the EGF. We perform this procedure on seismograms from all available stations for each mainshock.

Once we assemble a collection of RSTFs for an event (one for each available station) we stack over available RSTFs to improve the signal to noise ratio and eliminate uncertainties due to mechanism differences between the EGF and the mainshock (Velasco et al. 1994). Finally, we use the Orowan fault model to calculate the dynamic stress drop (e.g., Orowan, 1960; Velasco et al., 1994; Shearer, 2009; Escudero and Doser, 2012) from the RSTFs.

Results of the EGF analysis are given in Table 2 and shown in Figures 10 to 13. When more than one suitable EGF for a particular mainshock was available we selected the mainshock-EGF pair with more stations and/or the pair that best fulfills the EGF requirements (e.g. closest hypocenter, most similar focal mechanism).

Figure 10 shows stress drop values (stress drop labels keyed to Table 2) versus seismic moment. Over the moment range of 10^{18} to 10^{21} N-m the stress drop values are independent of moment, which implies self-similarity over this moment range, in agreement with Allmann and Shearer (2009). Sufficient data are not available for moments above 10^{21} N-m to make any conclusions regarding self-similarity for larger earthquakes. Note that stress drops estimated for the Nenana Mountain mainshock (estimates 021023E and 021023A) are 2 to 4 times greater than those estimated for the Denali fault (estimates 021103A and 021103B).

Previous studies (e.g. Escudero and Doser, 2012; Allmann and Shearer, 2009; Choy and Boatwright, 1995) have suggested that stress drop changes with focal mechanism type, with global analyses suggesting strike-slip events in oceanic plates have the largest observed stress drops. We parameterized the focal mechanism type (*fptype*) using the algorithm of Shearer et al.

(2006) and Allman and Shearer (2007). $f_{p\text{type}}$ varies from -1 (normal) to 0 (strike-slip) to 1 (reverse). Figure 11 shows a clear decreasing trend as $f_{p\text{type}}$ increases. That is, the stress drop values decrease going from pure strike-slip to reverse fault earthquakes.

Figure 12 suggests that stress drop decreased with increasing time over the two months following the Nenana Mountain mainshock. This is consistent with Allmann and Shearer's (2007) studies of temporal stress drop variations.

To examine the variation of stress drop along the strike of the Denali-Totschunda system we compare change in stress drop with longitude (Figure 13) as compared with horizontal and vertical surface fault offsets (middle figures) based on Eberhart-Phillips et al. (2003). Note that the highest stress drop events appear to occur at the ends of the surface rupture with the lowest stress drops occurring between longitudes 145° and 144° W. The gray box indicates the suspected rupture zone for the 1912 Delta River earthquake (Carver et al., 2004) along the Denali fault. Note that stress drops for the aftershocks located within the 1912 rupture zone have moderately high values (8-10 MPa). We still need to verify if differences in bedrock type along the fault could explain some of this observed variation stress drop, but the results do suggest interesting relationships between stress drop and offset along the Denali and Totschunda faults. Results of this work are in preparation for submission to the *Bulletin of Seismological Society of America*.

Related Studies

Previously funded NEHRP research projects on southeastern Alaska and the Chugach-St. Elias region have produced numerous results. A study of the general seismicity and tectonics of southeastern Alaska (Dixon Entrance to Yakutat Bay) was published by Doser and Rodriguez, (2011). A paper focusing on the aftershocks of the 1979 St. Elias earthquake sequence (Doser, 2012) has been accepted for publication in the *Bulletin of the Seismological Society of America*. A manuscript that examines the possible linkage between the Fairweather and Denali fault systems is in preparation for *Tectonophysics*. Studies of the stress drops of southeastern Alaska earthquakes using the empirical Greens function approach (Escudero and Doser, 2012) has also been accepted for publication in the *Bulletin of the Seismological Society of America*.

Oscar Romero, who was supported during his doctoral studies by NEHRP funds, has submitted a paper (Romero and Doser, 2012) to the *Bulletin of the Seismological Society of America* on stress drops of intraplate slab earthquakes in south-central Alaska. His results suggest that events occurring within the slab beneath the more strongly coupled portion of the plate interface have higher stress drops.

Reports Published

Schinagel, S.M., and D.I. Doser, Application of low-pass directional filtering techniques to aeromagnetic data in order to better determine relationships between seismicity and deep structure anomalies within central interior Alaska along the Denali fault, Geol. Soc. Amer. Rocky Mtn. Section Meeting, Albuquerque, NM, abstract 23-21, May 2012.

Dankoff, C.J., D.I. Doser and S.M. Schinagel, A study of historic earthquakes of interior Alaska's seismic zones, Geol. Soc. Amer. Rocky Mtn. Section Meeting, Albuquerque, NM, abstract 34-12, May 2012.

Doser, D.I., S. Schinagel and C. Dankoff, Integrating seismicity and potential fields data to determine structural controls on the Fairbanks and Salcha Seismic Zones, Interior Alaska, *Seismological Res. Lett.* 83, p.369, 2012.

Availability of Data Sets

Copies of digital/digitized seismograms used in this study may be obtained from Dr. Diane Doser, (915)-747-5851 or doser@ utep.edu. Gravity and magnetic data used in this study have been published by Saltus et al. (2006) and Saltus et al. (1999).

Bibliography

- Allmann, B. P., and P. M. Shearer, Spatial and temporal stress drop variations in small earthquakes near Parkfield, California, *J. Geophys. Res.*, 112, B04305, 2007.
- Allmann, B. P., and P. M. Shearer, Global variations of stress drop for moderate to large earthquakes, *J. Geophys. Res.*, 114, B01310, 2009.
- Ammon, C. J., A. A. Velasco, and T. Lay, Rapid estimation of rupture directivity: Application to the 1992 Landers ($M = 7.4$) and Cape Mendocino ($M_s = 7.2$) California earthquakes, *Geophys. Res. Lett.*, 20, 97–100, 1993.
- Brocher, T. M., G.S. Fuis, W.J. Lutter, N.I. Christensen, N.A. Ratchkovski, Seismic velocity models for the Denali fault zone along the Richardson Highway, Alaska, *Bull. Seism. Soc. Am.* 94, part B, S85-S106, 2004.
- Carver G., G. Plafker, M. Metz, L. Cluff, B. Slemmons, E. Johnson, J. Roddick, and S. Sorensen, Surface Rupture on the Denali Fault Interpreted from Tree Damage during the 1912 Delta River $M_w 7.2$ – 7.4 Earthquake: Implications for the 2002 Denali Fault Earthquake Slip Distribution. *Bull. Seism. Soc. Am.*, 94, 6B, S58–S71, 2004.
- Choy, G., and J. Boatwright, Global patterns of radiated seismic energy and apparent stress, *J. Geophys. Res.*, 100, 18,205–18,228, 1995.
- Doser, D.I., Revisiting the 1979 St. Elias, Alaska, aftershock sequence and its regional significance, in press, *Bull. Seismol. Soc. Am.* (to be published in December issue), 2012.
- Doser, D.I., and H. Rodriguez, A seismotectonic study of the southeastern Alaska region, *Tectonophysics* 497, 105-113, 2011.
- Ebel, J. E., K. P. Bonjer, and M.C. Oncescu, Paleoseismicity: seismicity evidence for past large earthquakes. *Seismol. Res. Lett.* 71, 283–294, 2000.
- Eberhart-Phillips, D., P. J. Haeussler, J. T. Freymueller, A. D. Frankel, C. M. Rubin, P. Craw, N. A. Ratchkovski, G. Anderson, G. A. Carver, A. J. Crone, T. E. Dawson, H. Fletcher, R. Hansen, E. L. Harp, R. A. Harris, D. P. Hill, S. Hreinsdottir, R. W. Jibson, L. M. Jones, R. Kayen, D. K. Keefer, C. F. Larsen, S. C. Moran, S. F. Personius, G. Plafker, B. Sherrod, K. Sieh, N. Sitar, W. K. Wallace, The 2002 Denali fault earthquake, Alaska: A large magnitude, slip-partitioned event, *Science*, 300, 1113–1118, 2003.
- Escudero, C.R., and D.I. Doser, Relative source time function studies and stress drop of earthquakes in southeastern Alaska-northwestern Canada, in press, *Bull. Seismol. Soc. Am.*, (to be published in October issue), 2012.
- Fletcher, H.J., and D. H. Christensen, A determination of source properties of large intraplate earthquakes in Alaska, *Pure and Appl. Geophys.* 146, 21-41, 1996.
- Gedney, L., and E. Berg, The Fairbanks earthquakes of June 21, 1967; aftershock distribution, focal mechanisms, and crustal parameters, *Bull. Seismol. Soc. Amer.* 59, 73-100, 1969.
- Gedney, L.D., S.A. Estes, N.N. Biswas, and D. L. Marshall, A note on further activity in the Fairbanks, Alaska, seismic zone, *Bull. Seismol. Soc. Amer.* 72, 1415-1417, 1982
- Gedney, L., S. Estes, and N. Biswas, Earthquake migration in the Fairbanks, Alaska, seismic zone, *Bull. Seismol. Soc. Amer.* 70, 223-241, 1980.

- Haeussler, P.J., et al., Surface rupture and slip distribution of the Denali and Totschunda faults in the 3 November 2002 M 7.9 earthquake, Alaska, *Bull. Seism. Soc. Am.* 94, S23-S52, 2004.
- Lee, W.H.K, and D.A. Dodge, Development of a direct search software package for locating poorly constrained earthquakes, *Seismol. Res. Lett.* 77, 292-292, 2006.
- Matmon, A., D.Schwartz, P. Haeussler, R. Finkle, J. Lienkaemper, H. Stenner, and T. Dawson, Denali fault slip rates and Holocene-late Pleistocene kinematics of central Alaska, *Geology* 34, 645-648, 2006.
- Mueller, C. S., Source pulse enhancement by the deconvolution of an empirical green's function., *Geophys. Res. Lett.*, 12, 33–36, 1985.
- Orowan, E., Mechanism of faulting, *Geol. Soc. Am.*, 79, 323–345, 1960.
- Shearer, P. M., *Introduction to Seismology*, Cambridge University Press, The Edinburgh Building, Cambridge CB2 8RU, UK, 2009.
- Page, R.A., G. Plafker, and H. Pulpan, Block rotation in east-central Alaska: A framework for evaluating earthquake potential? *Geology* 23, 629-632, 1995.
- Plafker, G., L.M. Gilpin, and J. C. Lahr, Neotectonic map of Alaska, in *The Geology of North America*, vol. G-1, *The geology of Alaska* (G. Plafker and H.C. Berg, eds.), *Geol. Soc. Amer.*, Boulder, Colo., pp. 389-449, 1994.
- Romero de la Cruz, O.M., Dynamic stress drop estimation from moderate earthquakes in south-central Alaska, submitted to *Bull. Seismol. Soc. Amer.*, March 2012.
- Ruppert, N.A., K.D. Ridgway, J.T. Freymueller, R.S. Cross, and R.A. Hansen, Active tectonics of interior Alaska: Seismicity, GPS geodesy, and local geomorphology, *American Geophysical Union Monograph* 179 on “Active Tectonics and Seismic Potential of Alaska”, J. T. Freymueller, P.J. Haeussler, R. Wesson and G. Ekstrom (eds.), 351-367, 2008.
- Saltus, R.W., P.J. Brown II, R.L. Morin, and P.L. Hill , *Compilation of Alaska Gravity Data and Historical Reports*, U.S. Geol. Surv. Data Series Report 264, 2006.
- Saltus, R.W., G.G. Connard and P.L. Hill, *Alaska Aeromagnetic Compilation-Digital Grids and Survey Data*, U.S. Geol. Surv. Open File Rept. 99-502, 1999.
- Shearer, P. M., G. A. Prieto, and E. Hauksson, Comprehensive analysis of earthquake source spectra in southern California, *J. Geophys. Res.*, 111, B06, 303, 2003
- Velasco, A.A., C.J. Ammon, and T. Lay, Empirical Green function deconvolution of broadband surface waves: rupture directivity of the 1992 Landers, California (M=7.3) earthquake, *Bull. Seism. Soc. Amer.* 84, 735-750, 1994.

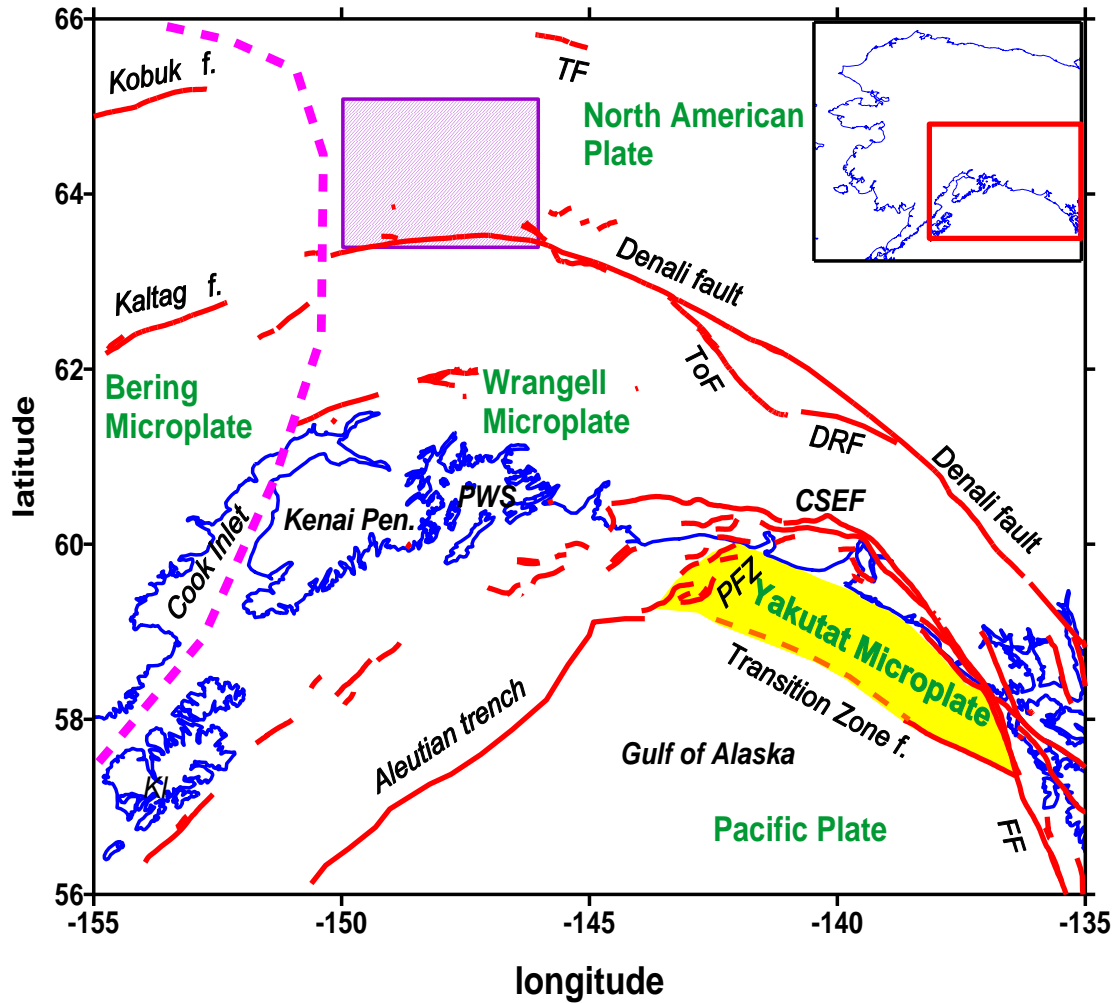


Figure 1 – Location of study area (purple box) relative to major tectonic features of south-central Alaska. Red lines are faults with Holocene or Pleistocene motion from Plafker et al. (2004). Yellow is exposed portion of Yakutat microplate. Bold dashed line is inferred edge of Bering microplate (Ruppert et al., 2008). CSEF is Chugach-St. Elias fault, DRF is Duke River fault, FF is Fairweather fault, PFZ is Pamplona fault zone, PWS is Prince William Sound, TF is Tintina fault, ToF is Totschunda fault.

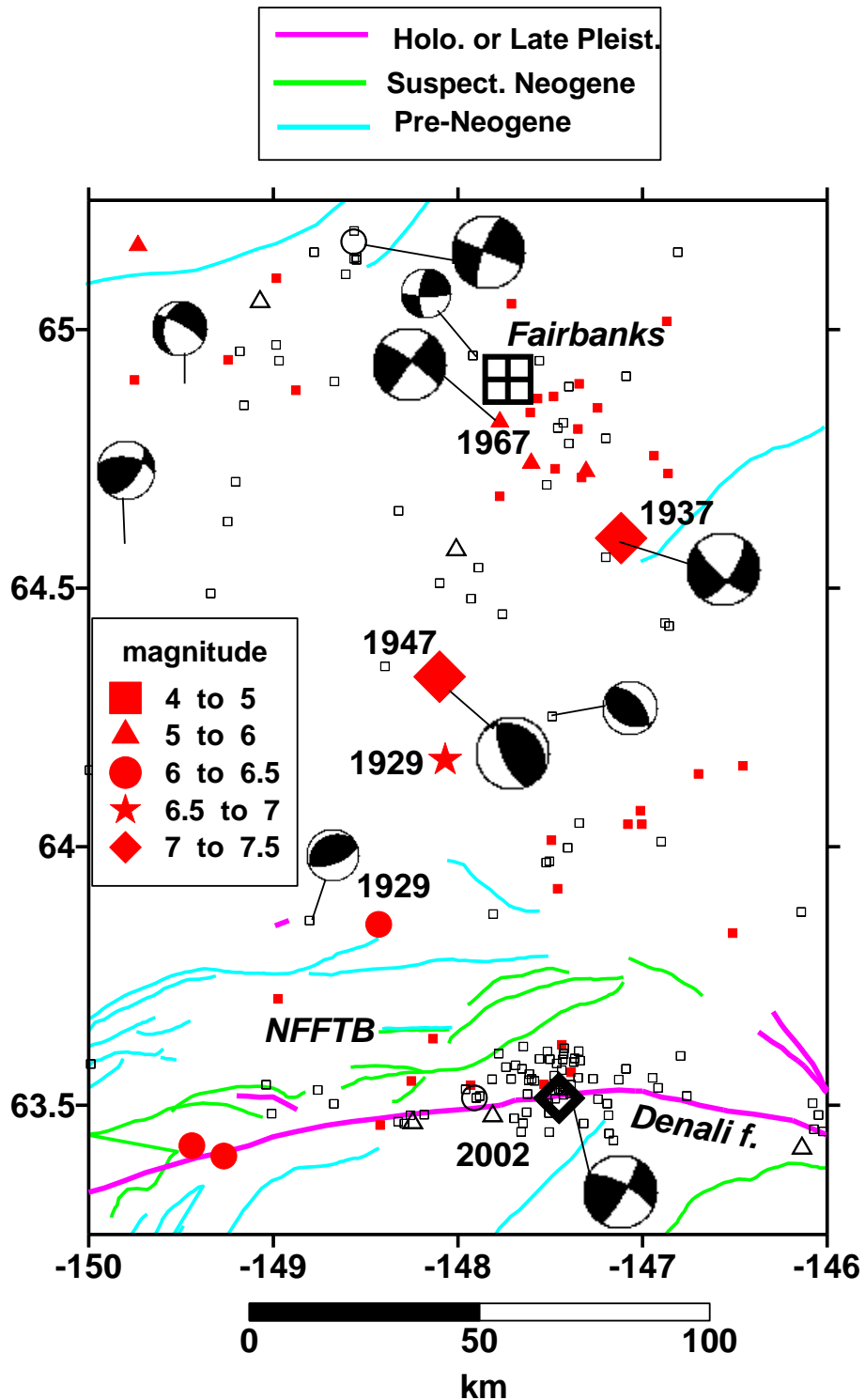


Figure 2- Relocated seismicity ($M > 4$) of the study area. Red solid symbols are events occurring prior to 1973 relocated using jloc (Lee and Dodge, 2006). Black open symbols are events occurring between 1973 and 2011 from the Alaska Earthquake Information Center. Square is Fairbanks. Colored lines represent faults as indicated (from Plafker et al., 1994). Large focal mechanisms indicate $M > 5.5$ events. Important historic events are labeled.

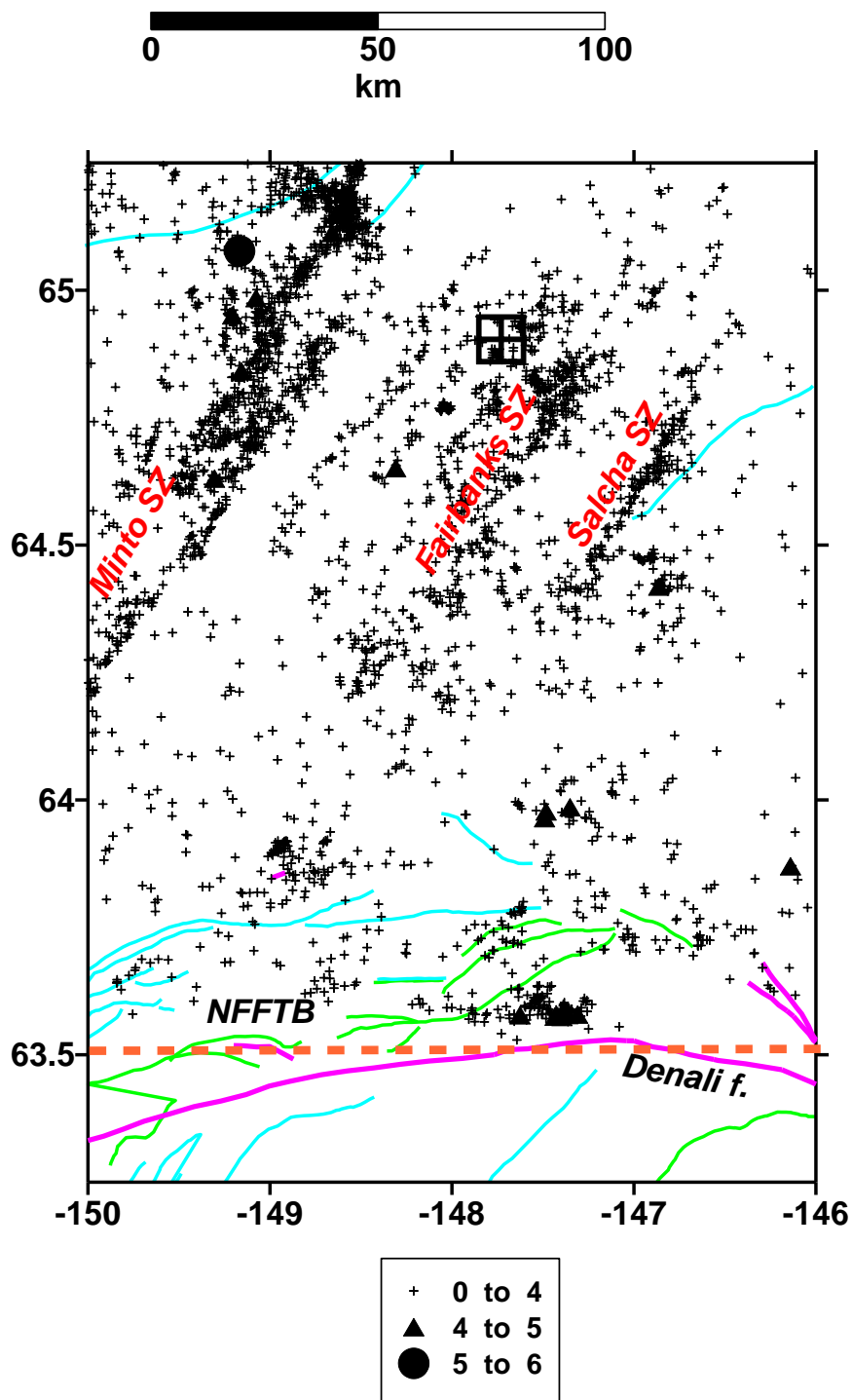


Figure 3 – Relocated seismicity from Rupert et al. (2008). Dashed line indicates edge of study area for relocations. The three prominent seismic zones are labeled. Square is Fairbanks.

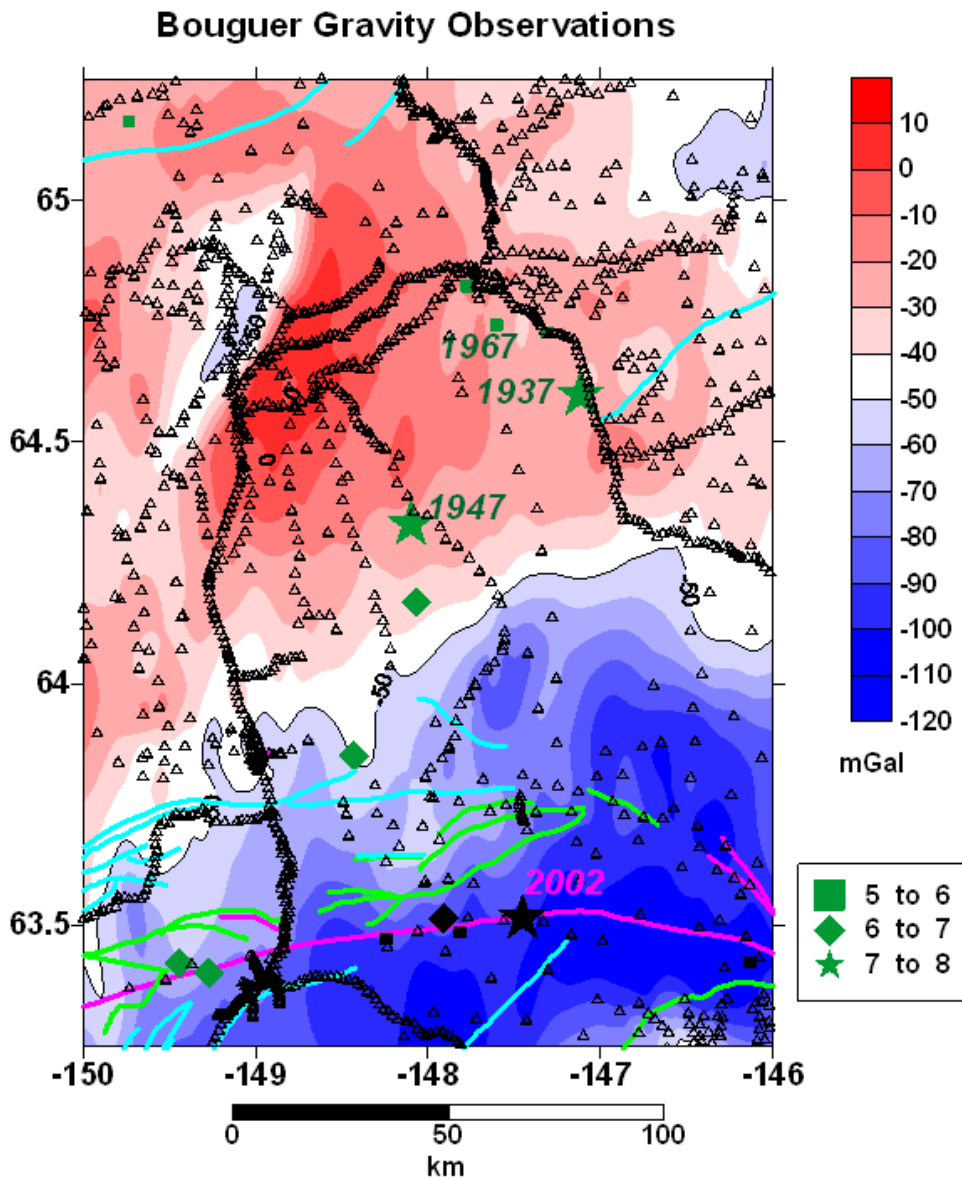


Figure 4 –Bouguer gravity anomaly map with location of gravity observations (triangles) and earthquakes of $M \geq 5$ (green and black solid symbols). Gravity data from Saltus et al. (2006). Contour lines for -50 mGal Bouguer anomaly are indicated with fine black lines.

Bouguer Gravity and Seismicity

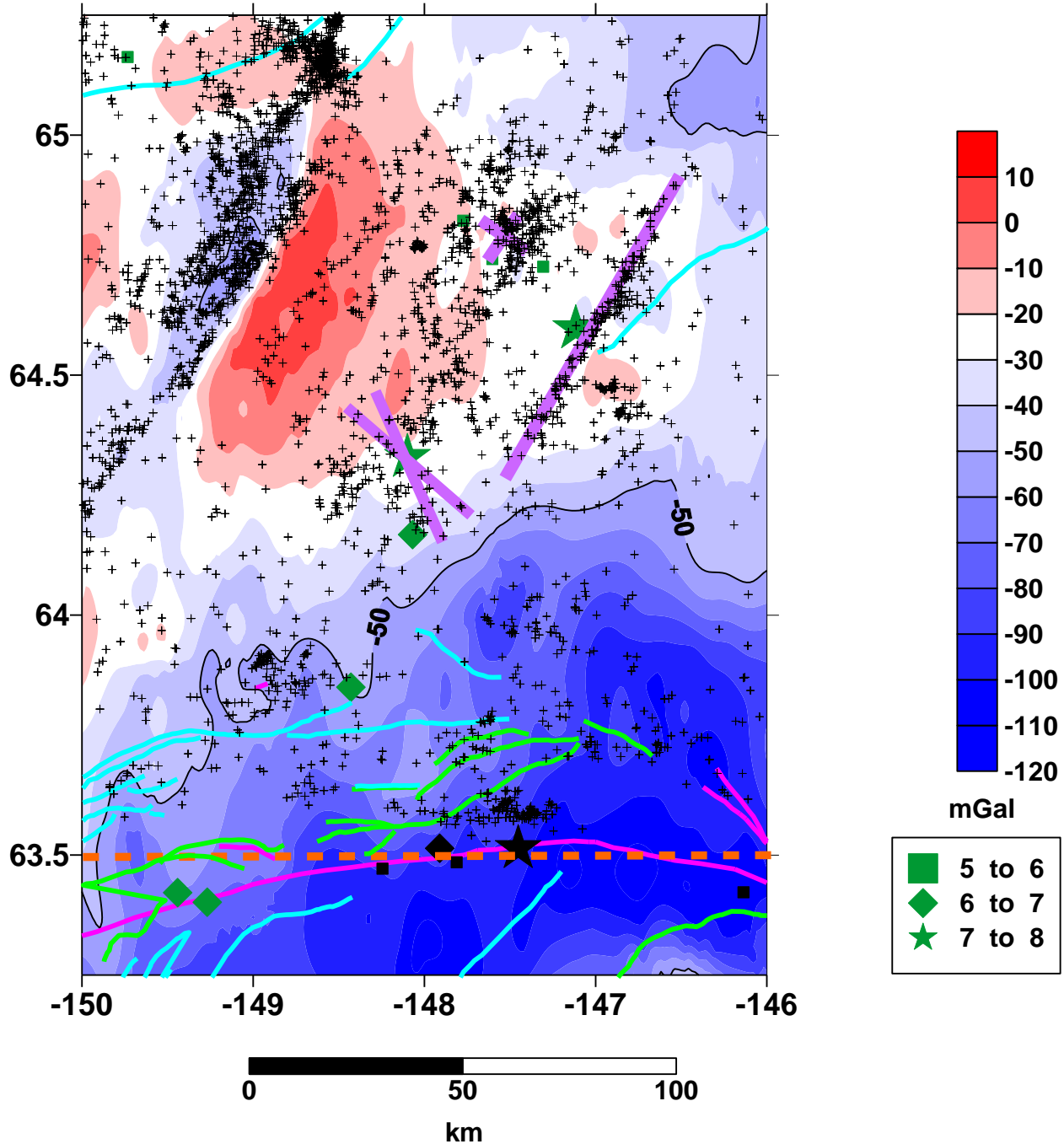


Figure 5- Bouguer gravity anomaly compared to seismicity. Earthquake symbols for $M \geq 5$ events are the same as shown in Figure 4. Plus symbols are the relocations from Rupert et al. (2008). Purple bold lines indicated estimated rupture lengths for the 1937 Salcha and 1947 Fairbanks earthquakes from Fletcher and Christensen (1996) (based on waveform modeling results and nodal plane orientations) and the 1967 Fairbanks events (based on their magnitudes and nodal plane orientations).

Aeromagnetics and Seismicity

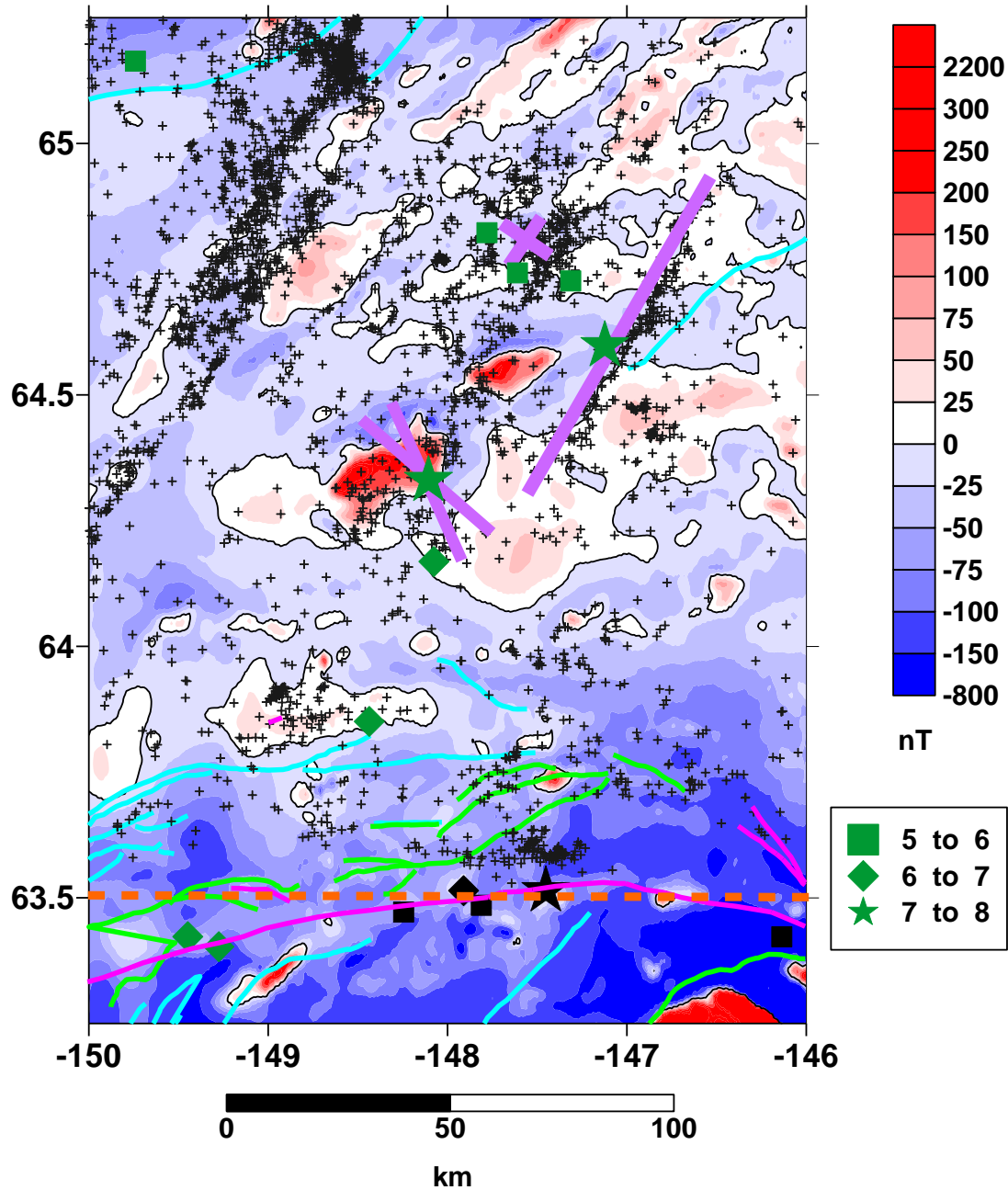


Figure 6 – Aeromagnetic intensity map of study area (data from Saltus et al., 2009) compared to seismicity. Symbols are the same as Figures 4 and 5. Zero nT magnetic contours are indicated by fine black lines.

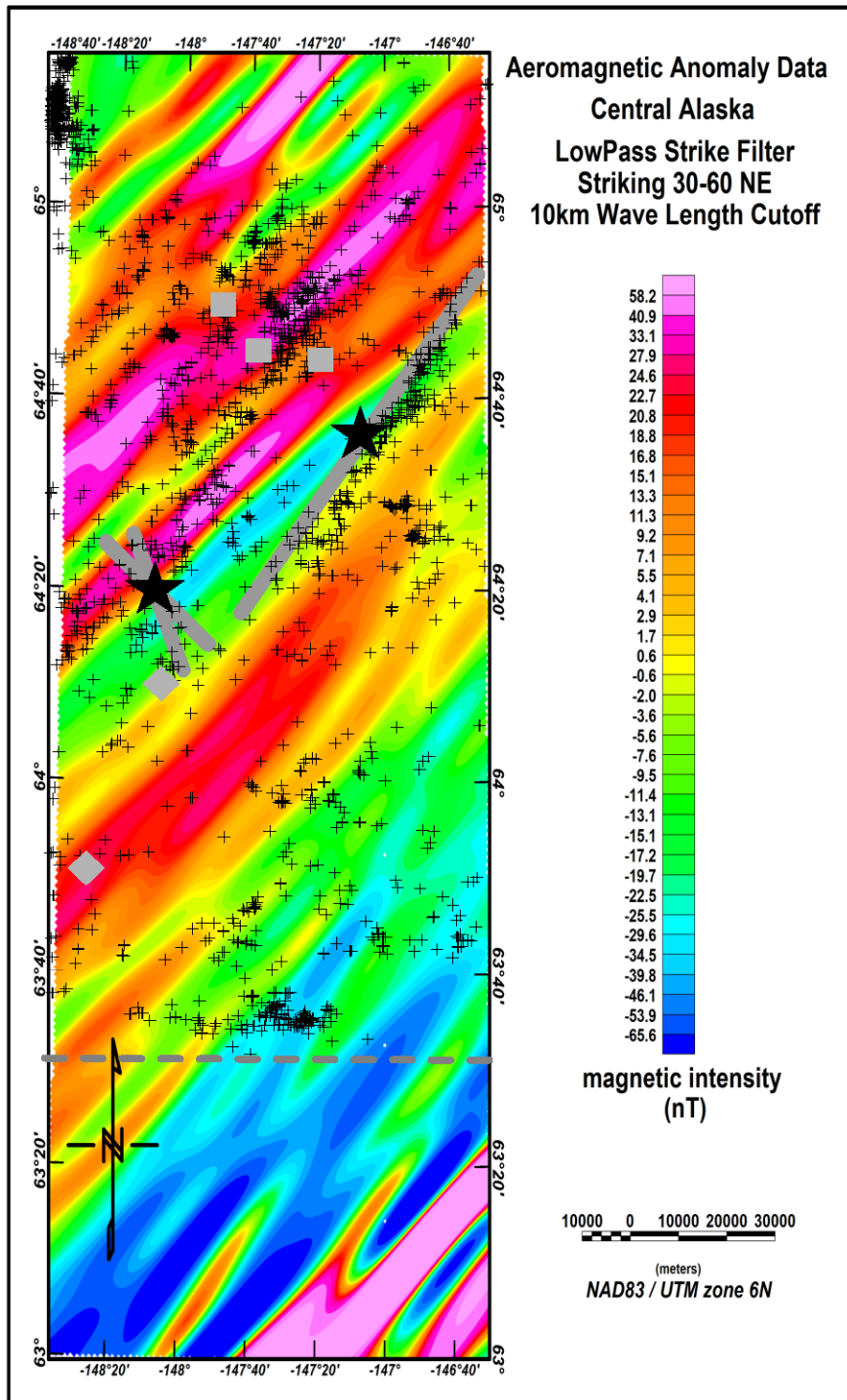


Figure 7- Filtered magnetic intensity map for region between Fairbanks and Salcha seismic zones. Data have been low pass filtered (wavelengths > 10 km passed) and strike filtered (features striking 30 to 60 degrees NE passed). Gray solid lines indicate inferred rupture zones. Symbols are the same as in previous figures.

Aeromagnetics (shaded relief) and Gravity (color)

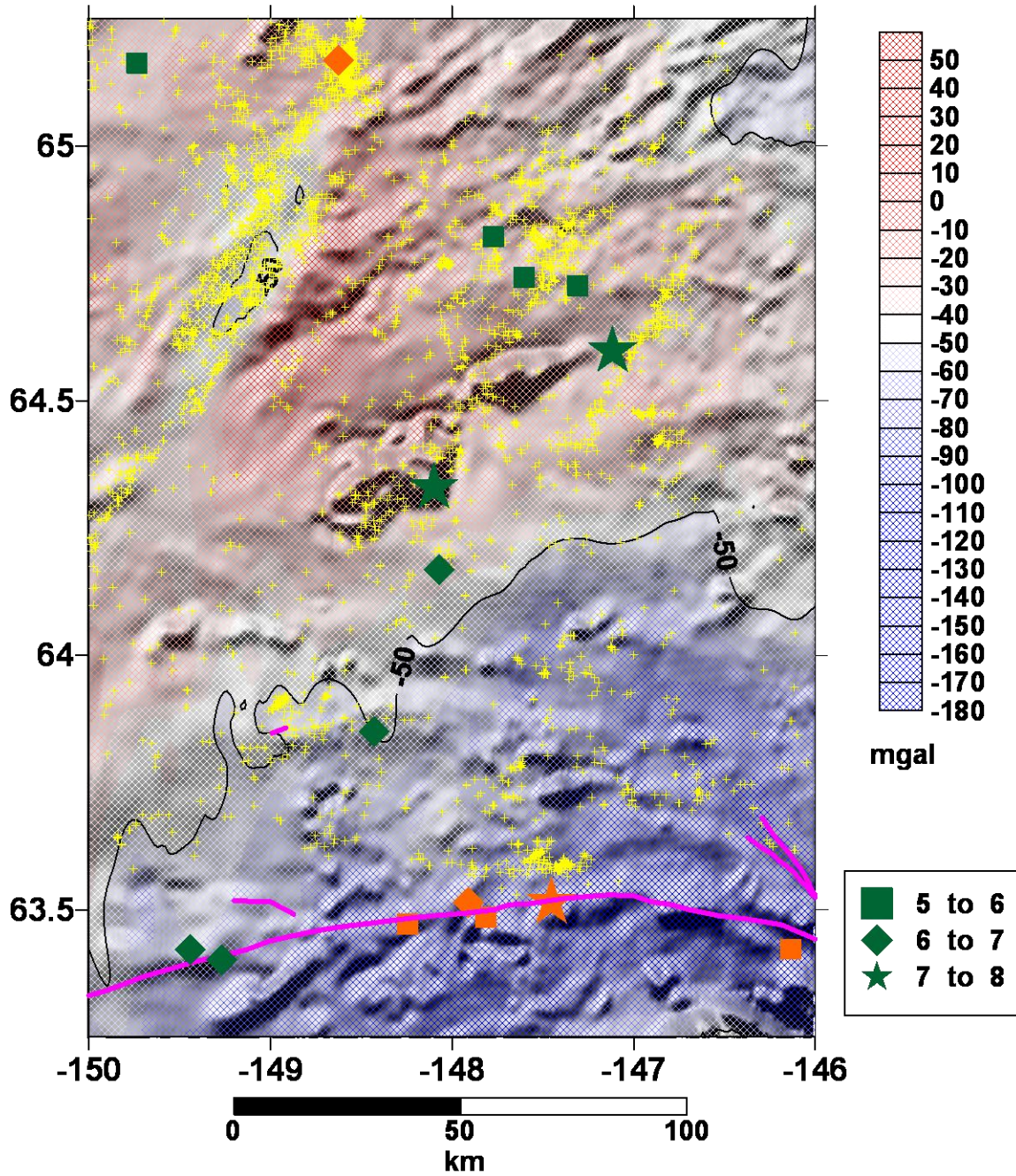


Figure 8 – Shaded relief map of magnetic intensities draped with colored map of Bouguer gravity anomaly. This helps to highlight basement features that may be related to seismicity. -50 mGal Bouguer gravity anomaly contours indicated by fine black lines.

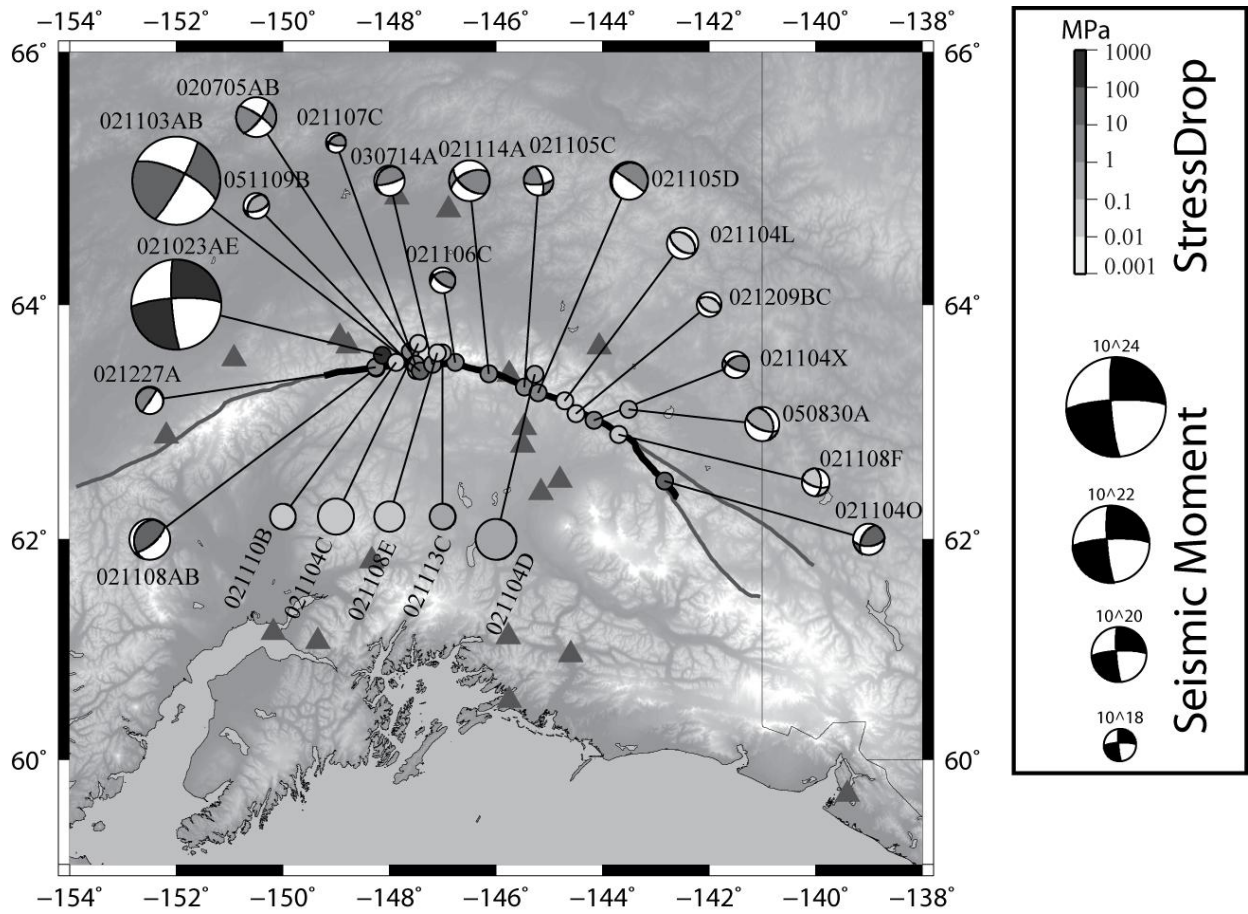


Figure 9 – Location of earthquakes examined in empirical Greens function study. Stations are indicated by triangles. Dot color is scaled to earthquake stress drop (top right scale). Focal mechanism size is scaled to seismic moment (bottom right scale). Blank labeled circles indicate events where no focal mechanism information was available. Labels are keyed to Table 2. Gray lines indicate traces of Denali and Totschunda faults. Thin line is U.S.-Canadian border.

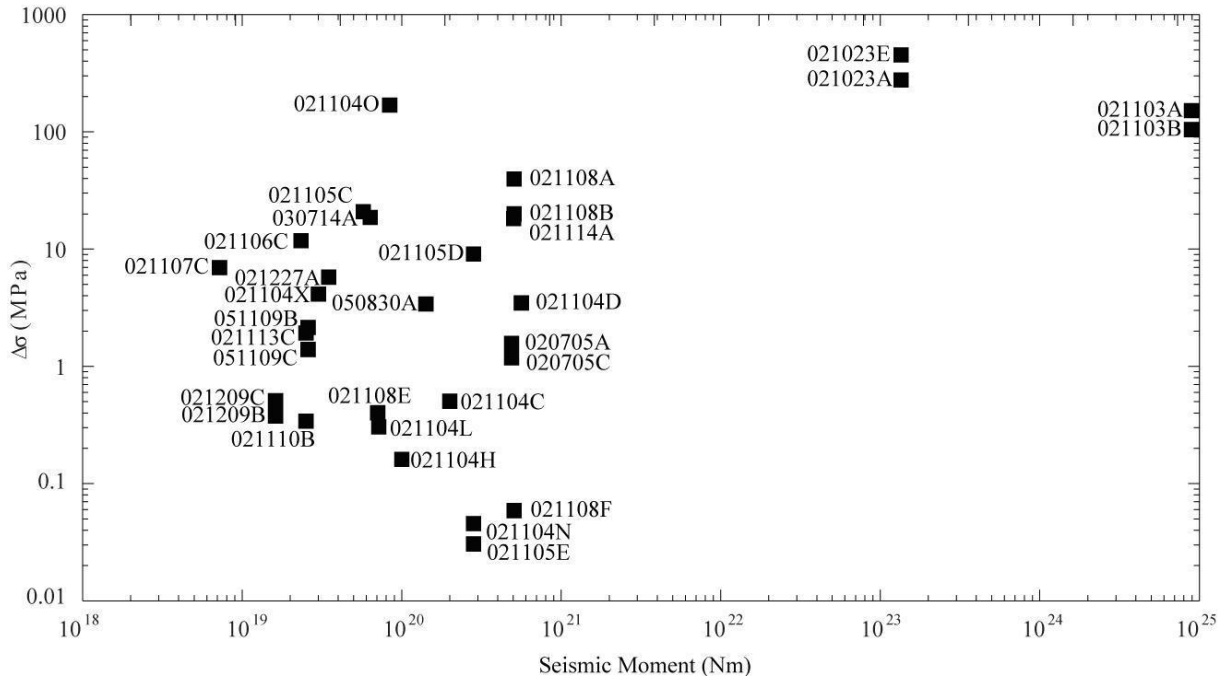


Figure 10 – Stress drop compared to seismic moment. Labels keyed to Table 2.

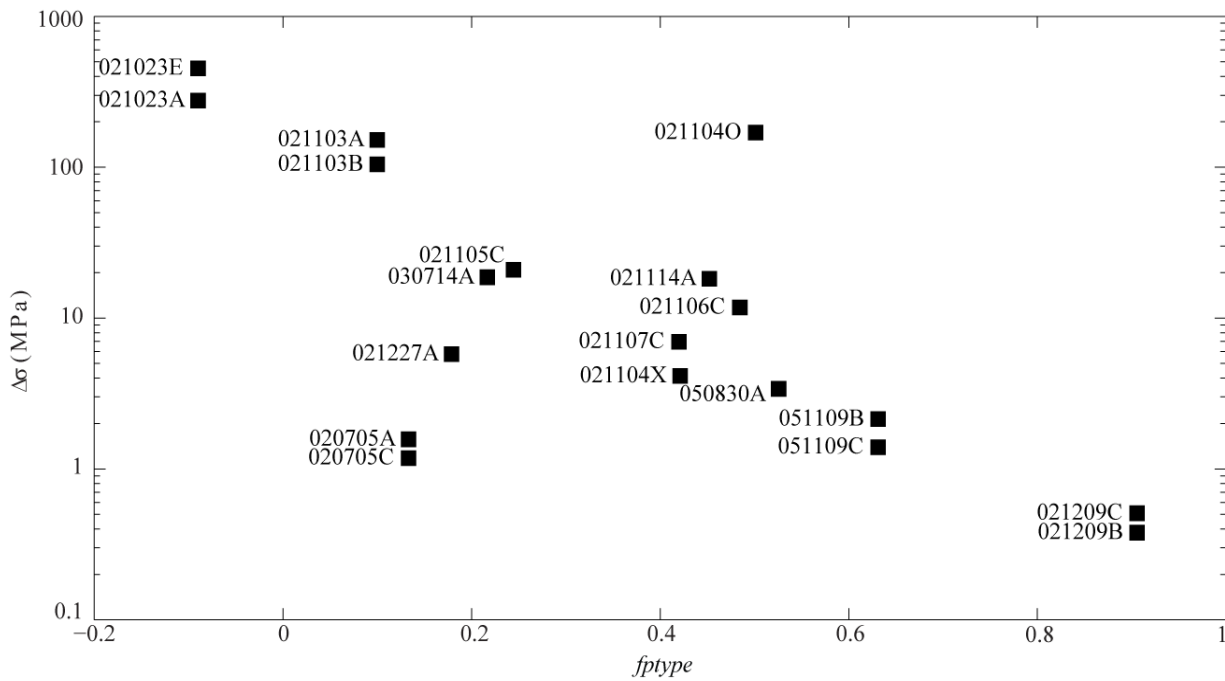


Figure 11- Stress drop versus $f_{p\text{type}}$ (see text for description).

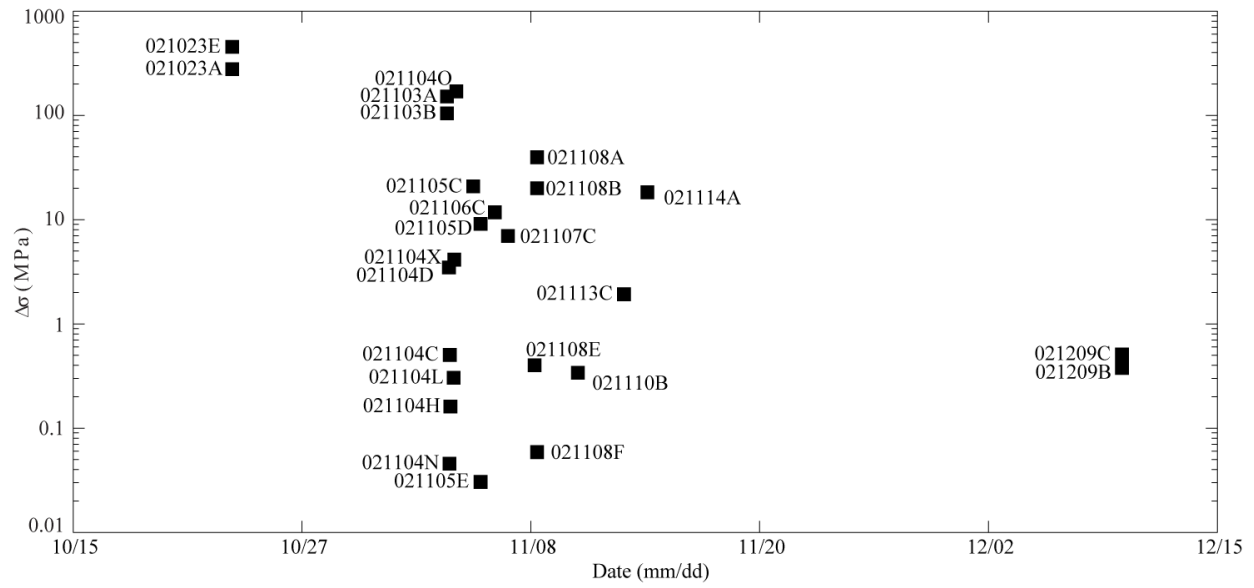


Figure 12 – Stress drop versus time (starting October 15, 2002 and ending December 15, 2002).

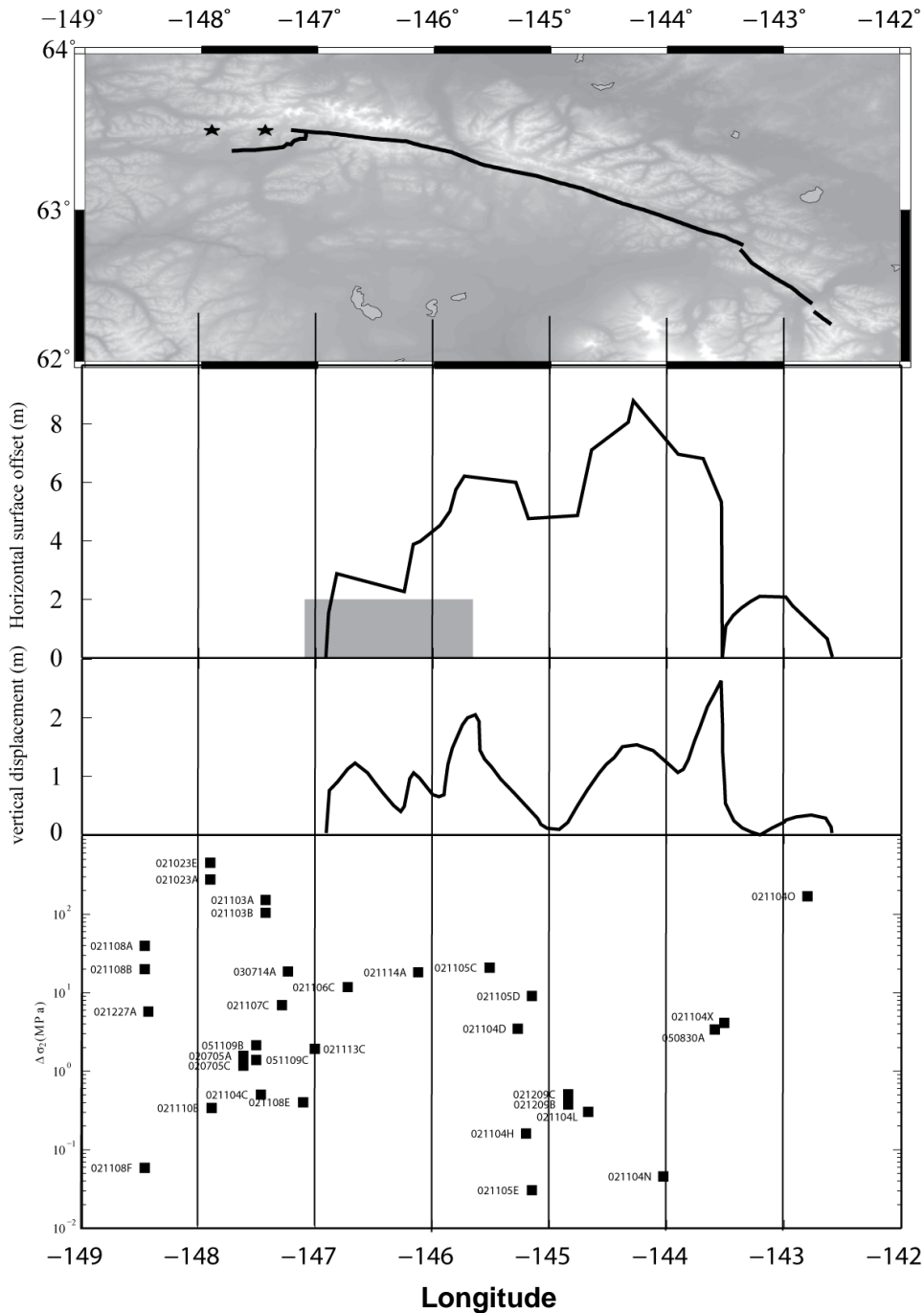


Figure 13- Stress drop versus position along Denali-Totschunda fault system. Top map shows fault rupture in 2002 and locations of Nenana Mountain and Denali fault mainshocks (stars). Top plot shows horizontal offset along main rupture zone in meters (from Eberhart-Phillips et al., 2003). Gray square is estimated rupture zone for 1912 Delta River earthquake along the Denali fault (Carver et al., 2004). Middle plot shows vertical offset along main rupture zone. Lower plot shows stress drop as a function of longitude.

Table 1. Source parameters of earthquakes analyzed in this study

Date yr/mo/day	Time hr:min:sec	Long (°)	Lat (°)	M _L	*M ₀ (M _L) (N-m)	M _w	M ₀ (N-m)
2002-07-05	16:41:41	-147.61	63.61	4.9	-	5.1	4.89x10 ¹⁹
2002-10-23	11:27:18	-148.21	63.56	6.2	-	6.7	1.35x10 ²⁴
2002-11-03	22:12:42	-147.42	63.71	5.2	-	7.9	8.91x10 ²³
2002-11-04	00:50:44	-145.27	63.42	5.1	5.62x10 ¹⁹	-	-
2002-11-04	01:38:54	-144.03	63.25	4.9	2.82x10 ¹⁹	-	-
2002-11-04	01:53:37	-147.46	63.68	4.8	2.00x10 ¹⁹	-	-
2002-11-04	02:38:06	-145.20	63.30	4.6	1.00x10 ¹⁹	-	-
2002-11-04	06:50:18	-144.67	63.28	4	-	4.5	7.17x10 ¹⁸
2002-11-04	07:43:25	-143.51	62.81	5	-	4.3	3.01x10 ¹⁸
2002-11-04	10:15:15	-142.80	62.50	3.5	-	4.6	8.42x10 ¹⁸
2002-11-04	22:45:45	-145.28	63.32	3.9	8.91x10 ¹⁷	-	-
2002-11-05	07:50:47	-145.51	63.41	4.9	-	4.5	5.74x10 ¹⁸
2002-11-05	14:33:22	-142.97	62.67	4.7	-	4.8	1.55x10 ¹⁹
2002-11-05	17:22:41	-145.15	63.38	4.9	2.82x10 ¹⁹	-	-
2002-11-06	11:41:13	-146.72	63.60	4.1	-	4.2	2.34x10 ¹⁸
2002-11-07	04:18:59	-147.28	63.29	4	-	3.8	7.20x10 ¹⁷
2002-11-07	22:07:56	-145.29	63.32	4.2	-	4	1.28x10 ¹⁸
2002-11-08	14:24:45	-147.10	63.60	4.5	7.08x10 ¹⁸	-	-
2002-11-08	17:34:53	-148.45	63.56	5	-	5.1	5.07x10 ¹⁹
2002-11-08	17:54:23	-143.60	62.98	4.4	-	4.4	3.92x10 ¹⁸
2002-11-08	18:21:20	-144.17	63.12	3.8	6.31x10 ¹⁷	-	-
2002-11-08	20:29:00	-143.48	62.93	5	-	5	3.48x10 ¹⁹
2002-11-08	20:29:03	-143.56	62.90	4.8	-	5	3.48x10 ¹⁹
2002-11-09	01:14:04	-147.42	63.61	4.1	1.78x10 ¹⁸	-	-
2002-11-10	05:35:53	-148.03	63.53	4.2	-	3.8	5.51x10 ¹⁷
2002-11-10	21:49:42	-147.88	63.52	4.2	2.51x10 ¹⁸	-	-
2002-11-13	08:39:12	-147.00	63.60	4.2	2.51x10 ¹⁸	-	-
2002-11-14	14:37:24	-146.12	63.51	5.1	-	5.1	5.03x10 ¹⁹
2002-11-18	07:50:13	-147.65	63.50	4.2	-	4	9.67x10 ¹⁷
2002-11-18	20:21:32	-147.54	63.62	4	-	4	9.88x10 ¹⁷
2002-12-09	21:57:56	-144.84	63.22	4.1	-	4.1	1.62x10 ¹⁸
2002-12-14	16:27:35	-145.06	63.50	4.2	2.51x10 ¹⁸	-	-
2002-12-27	05:02:18	-148.42	63.56	4.1	-	4.3	3.49x10 ¹⁸
2003-03-03	12:12:52	-145.04	63.46	3.6	3.16x10 ¹⁷	-	-
2003-03-09	10:17:41	-147.69	63.68	4	-	4	9.94x10 ¹⁷
2003-03-30	13:41:23	-148.14	63.60	4.3	-	4.4	4.02x10 ¹⁸
2003-05-16	11:54:53	-147.63	63.63	3.7	4.47x10 ¹⁷	-	-
2003-07-14	15:50:49	-147.23	63.54	4.7	-	4.5	6.34x10 ¹⁸
2003-07-25	08:29:45	-148.13	63.48	4.1	-	4.3	3.18x10 ¹⁸
2003-11-02	19:27:01	-147.51	63.97	4.2	-	4.1	1.73x10 ¹⁸
2003-12-15	08:23:34	-143.62	62.90	4.3	-	4.1	1.58x10 ¹⁸
2004-02-28	23:31:32	-147.19	63.53	3.3	1.12x10 ¹⁷	-	-
2005-08-30	04:24:03	-143.59	63.18	4.6	-	4.7	1.42x10 ¹⁹

2005-11-09	07:17:07	-147.50	63.56	4.2	-	4.2	2.59x10 ¹⁸
2006-01-20	18:37:34	-143.39	63.10	3.7	4.47x10 ¹⁷	-	-
2007-05-24	19:27:56	-147.24	63.64	4.1	1.78x10 ¹⁸	-	-
*M _o (M _L) is the moment (M _o)determined from M _L (local magnitude) using the relationship M _L =log M _o /1.5 - 10.73							

Table 2. Mainshocks-EGF pairs and stress drop estimates

Label	Mainshock yr/mo/day hr:min:ss	EGF rr/mo/day hr:min:ss	M _w or M _L *	Δσ (MPa)
020705A	2002/07/05 16:41:41	2002/11/18 07:50:13	5.1/4	1.57
020705C	2002/07/05 16:41:41	2002/11/18 20:21:32	5.1/4	1.18
021023A	2002/10/23 11:27:18	2002/11/08 17:34:53	6.7/5.1	277.04
021023E	2002/10/23 11:27:18	2003/07/25 08:29:45	6.7/4.3	453.16
021103A	2002/11/03 22:12:42	2003/07/14 15:50:49	7.9/4.5	151.75
021103B	2002/11/03 22:12:42	2002/11/04 01:53:37	7.9/4.8L	104.39
021104D	2002/11/04 00:50:44	2002/12/14 16:27:35	5.1L/4.2L	3.47
021104N	2002/11/04 01:38:54	2002/11/08 18:21:20	4.9L/3.8L	0.046
021104C	2002/11/04 01:53:37	2002/11/09 01:14:04	4.8L/4.1L	0.50
021104H	2002/11/04 02:38:06	2003/03/03 12:12:52	4.6L/3.6L	0.16
021104L	2002/11/04 06:50:18	2002/11/04 22:45:45	4.5/3.9L	0.30
021104X	2002/11/04 07:43:25	2003/12/15 08:23:34	5L/4.1	4.13
021104O	2002/11/04 10:15:15	2002/11/05 14:33:22	4.6/4.8	169.62
021105C	2002/11/05 07:50:47	2002/11/04 22:45:45	4.5/3.9L	20.85
021105D	2002/11/05 17:22:41	2002/12/14 16:27:35	4.9L/4.2L	9.09
021105E	2002/11/05 17:22:41	2003/03/03 12:12:52	4.9L/3.6L	0.03
021106C	2002/11/06 11:41:13	2002/11/09 01:14:04	4.2/4.1L	11.76
021107C	2002/11/07 04:18:59	2002/11/09 01:14:04	4.1L/4.1L	6.96
021108E	2002/11/08 14:24:45	2002/11/09 01:14:04	4.5L/4.1L	0.40
021108A	2002/11/08 17:34:53	2002/11/10 05:35:53	5.1/3.8	39.57
021108B	2002/11/08 17:34:53	2003/07/25 08:29:45	5.1/4.3	19.96
021108F	2002/11/08 17:34:53	2003/12/15 08:23:34	5.1/4.1	0.059
021110B	2002/11/10 21:49:42	2003/03/09 10:17:41	4.2L/4	0.34
021113C	2002/11/13 08:39:12	2002/11/09 01:14:04	4.2L/4.1L	1.92
021114A	2002/11/14 14:37:24	2002/11/09 01:14:04	5.1/4.1L	18.24
021209B	2002/12/09 21:57:56	2002/11/04 22:45:45	4.1/4.8L	0.37
021209C	2002/12/09 21:57:56	2003/03/03 12:12:52	4.1/3.6L	0.50
021227A	2002/12/27 05:02:18	2003/07/25 08:29:45	4.3/4.3	5.76
030714A	2003/07/14 15:50:49	2007/05/24 19:27:56	4.5/4.1L	18.63
050830A	2005/08/30 04:24:03	2003/12/15 08:23:34	4.7/4.1	3.39
051109B	2005/11/09 07:17:07	2003/03/09 10:17:41	4.2/4	2.14
051109C	2005/11/09 07:17:07	2002/11/18 20:21:32	4.2/4	1.39

*First value is magnitude for “mainshock” of EGF pair, second value is magnitude for EGF. “L” indicates local magnitude (M_L) value was used since no moment-magnitude (M_w) estimate was available.